

1 **Identification of a Short-Lived Strombolian or Vulcanian Thermal Event at Marduk**
2 **Fluctus, Io, using *Galileo* NIMS Data**

3
4 **A. G. Davies¹, R. L. Davies², G. J. Veeder³, K. de Kleer⁴, I. de Pater⁵, D. L. Matson³, T. V.**
5 **Johnson¹ and L. Wilson⁶**

6 1. Jet Propulsion Laboratory-California Institute of Technology, Pasadena, CA, USA

7 2. Oxted School, Bluehouse Lane, Oxted, Surrey, UK.

8 3. Bear Fight Institute, Winthrop, WA, USA.

9 4. California Institute of Technology, Pasadena, CA, USA.

10 5. University of California Berkeley, Berkeley, CA, USA.

11 6. Lancaster University, Lancaster, Lancashire, UK.

12 Corresponding author: Ashley Davies (Ashley.Davies@jpl.nasa.gov)

13
14
15 **Key Points:**

- 16 • We identify a powerful, short-lived thermal event in the vicinity of Marduk Fluctus in
17 *Galileo* NIMS Io data.
- 18 • The temporal evolution of this event is consistent with an explosion, with rapid cooling
19 suggesting the generation of small clasts.
- 20 • Similar events imaged from spacecraft will constrain lava eruption temperature if data are
21 obtained simultaneously at multiple wavelengths.
22

23 **Abstract**

24 Analysis of *Galileo* Near Infrared Mapping Spectrometer (NIMS) observations of Marduk
25 Fluctus, a volcano on the jovian moon Io, reveals a style of volcanic activity not previously seen
26 there – a powerful thermal event lasting only a few minutes. The thermal emission rapidly fades,
27 suggesting extremely rapid cooling of small clasts. The duration and evolution of the eruption is
28 akin to what might be expected from a strombolian or vulcanian explosion. The presence of
29 such events provides an additional volcanic process that can be imaged with the intent of
30 determining lava composition from eruption temperature, an important constraint on the internal
31 composition of Io. These data promise to be of particular use in understanding the mechanics of
32 explosive volcanic processes on Io.

33

34 **1 Introduction**

35 The highly-volcanic jovian moon Io exhibits many different modes of eruption and emplacement
36 of lava onto the surface (e.g., Davies, 2007; Davies et al., 2010). Observed and implied styles of
37 eruption are similar to those seen on terrestrial basalt volcanoes (active, overturning lava lakes;
38 pahoehoe-like insulated flows; open-channel flows; lava fountaining) (Davies, 2007). Ionian
39 volcanic activity is typically on much larger areal and volumetric scales than contemporary
40 terrestrial eruptions. Observations of thermal emission from Io's erupting volcanoes can be used
41 to constrain the composition of Io's lavas (Davies et al., 2001; 2017; McEwen et al., 1998). This
42 is important as the composition of the erupting lava reflects the degree of melting in the upper
43 mantle (Keszthelyi et al., 2007), which is a direct consequence of the depth and magnitude of
44 tidal heating due to the Laplace resonance. However, only eruption styles that reveal relatively
45 large areas at temperatures very close to the eruption temperature are suitable for this purpose.
46 The best targets for instruments on spacecraft flying close to Io include targets such as the bases
47 of lava fountains (Keszthelyi et al., 2001) and the lava stream within a lava tube as viewed
48 through a skylight (Davies et al., 2016). *Galileo* Near Infrared Mapping Spectrometer (NIMS)
49 data obtained in 1997 but only recently examined in detail reveal another process that may be
50 used for determining eruption temperatures: transient, short-wavelength thermal events
51 reminiscent of a large eruption on Io's surface. Such an event was observed at or near to the
52 active volcano Marduk Fluctus.

53

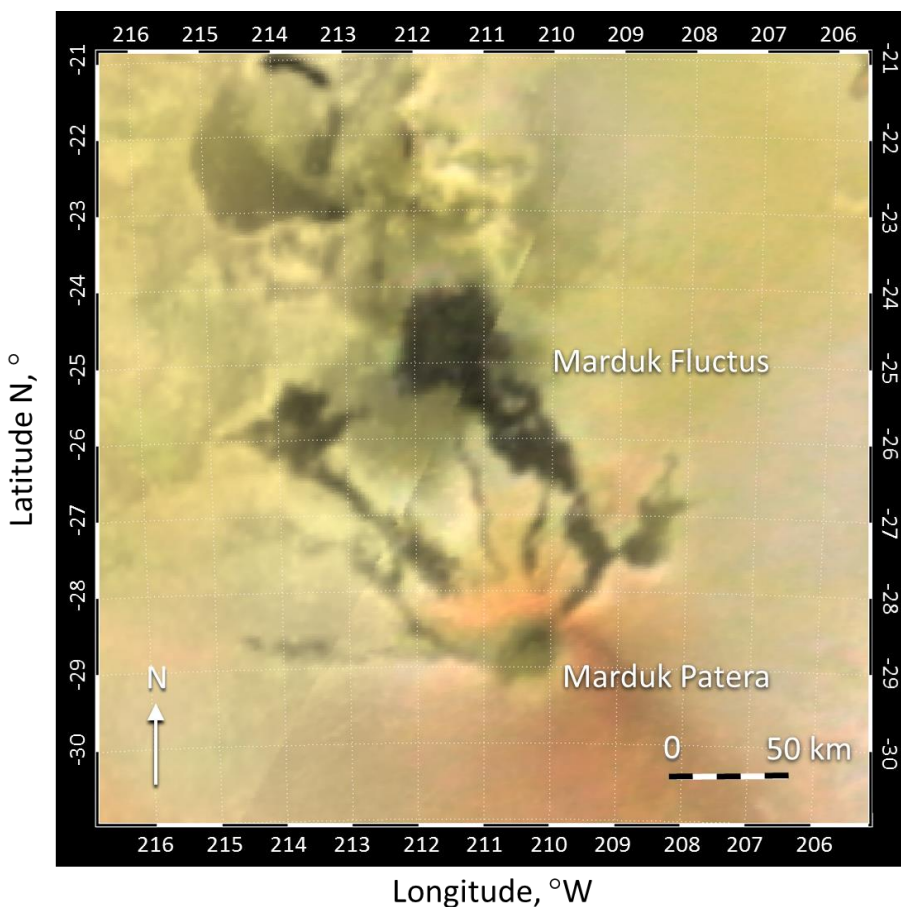
54 **2 Observations**

55 2.1 *Galileo* NIMS and observations of Io

56 The *Galileo* NIMS instrument (Carlson et al., 1992) was well-suited to measuring the
57 thermal emission from Io's volcanoes, as the 0.7 to 5.2 μm wavelength range meant that NIMS
58 was sensitive to surface temperatures from ~ 220 K to >1000 K (Davies et al., 2010). The

59 acquisition and processing of the high-precision NIMS radiance data is described in detail by
 60 Davies (2007). NIMS obtained 190 Io observations between 1996 and 2001. 27 observations of
 61 Io were obtained during *Galileo* orbit E4 between 17 and 19 December 1997. Many of these
 62 observations were designed to look for short-term variations in volcanic thermal emission. Six
 63 observations of Io obtained on 18 and 19 December 1997 covered much of the trailing
 64 hemisphere of Io (180° W to 360° W), including the location of Marduk Fluctus (209.9° W,
 65 28.4° S), a powerful and persistent volcano. Planetary Data System NIMS raw radiance “tube”
 66 products were used to measure radiance, and “cube” products, which have improved navigation,
 67 to identify hot spots (e.g., Davies et al., 2012).

68 2.1.1 Marduk Fluctus

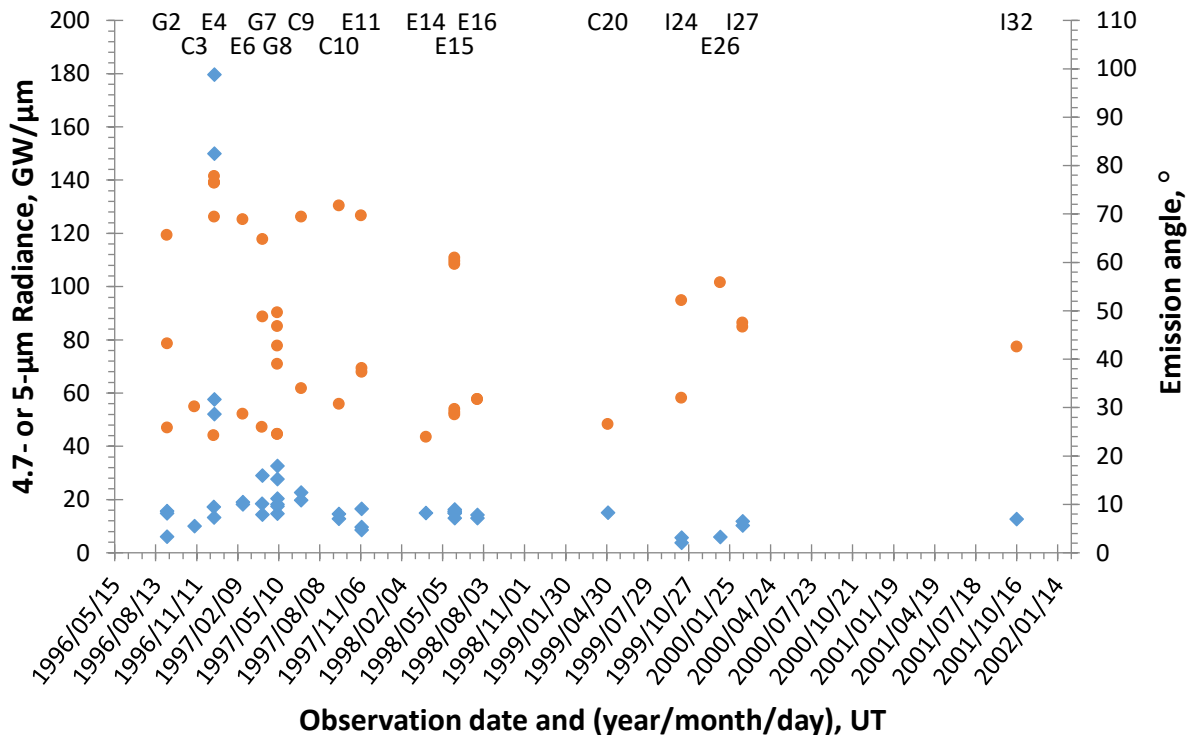


69

70 **Figure 1.** The Marduk Fluctus volcanic complex as seen by the *Galileo* Solid State Imaging
 71 experiment. Flows originate in a patera (a caldera-like volcanic depression) in the south of the
 72 image and flow northwards. The reddish deposit is rich in sulfur. This image is taken from the
 73 Io global mosaic of Becker and Geissler (2005).

74 Marduk Fluctus (Figure 1) has an extensive flow field identified early in the *Galileo* mission at
 75 Jupiter as a thermal source by both the *Galileo* Solid-State Imaging experiment (SSI)

76 (observation G1ISIOECLI02) (Belton et al., 1996; McEwen et al., 1997) and NIMS (Lopes-
 77 Gautier et al., 1997). The Marduk region was identified as a plume source in 1979 *Voyager* data
 78 (Strom et al., 1981), and SSI observed changes between the first two *Galileo* orbits in 1996.
 79 Marduk Fluctus has been identified as a thermal source in ground-based telescope data (e.g., de
 80 Pater et al., 2014b). SSI data show Marduk Fluctus as consisting of a series of at least six lava
 81 flows emanating from a patera and likely flowing downslope, consistent with the flows spreading
 82 laterally into a broad fan as the gradient decreases. Around the vent is a reddish plume deposit,
 83 likely rich in short-chain sulfur allotropes. The presence of these short-lived deposits is an
 84 indication of ongoing high-temperature (silicate) volcanic activity. The area is marked by what
 85 are presumably older flows which have cooled to the point where sulfur and SO₂ condense on the
 86 surface, yielding higher albedos than the active flows. The area of the young, black lava flows is
 87 $\approx 3600 \text{ km}^2$ (Veeder et al., 2009; 2012).



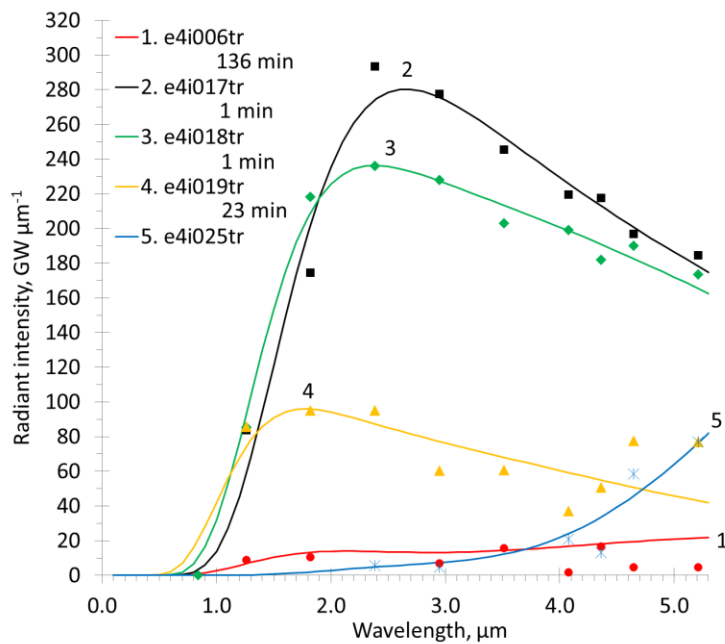
88

89 **Figure 2.** 4.7 or 5 μm radiances (blue diamonds), which are corrected for emission angle (angles
 90 shown as red circles) from NIMS observations that include Marduk Fluctus. *Galileo* orbit
 91 designations are also shown. The orbit E4 radiance values are unmatched, even in other
 92 observations taken at high emission angles.

93

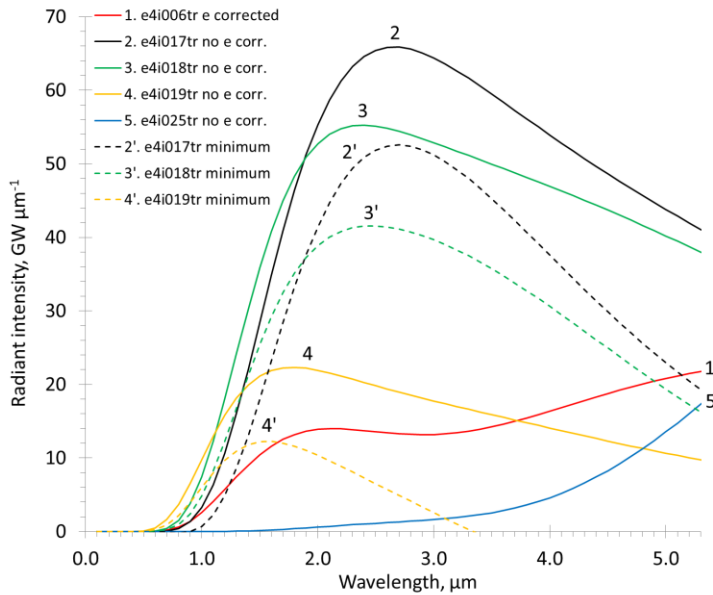
94 2.1.2 Marduk Fluctus E4 NIMS observations

95 Between 1996 and 2001 NIMS obtained 44 Io observations that included Marduk Fluctus. Six
 96 E4 observations (see Table 1) were obtained where thermal emission was detected from Marduk
 97 Fluctus on 18 and 19 December 1997. Marduk Fluctus was in darkness in the five latter
 98 observations, which were made on the outbound portion of *Galileo's* orbit. At a range of
 99 319,480 km, spatial resolution was 160 km/pixel for the first, day-lit observation (e4i007tr),
 100 which had an emission angle of 24.3°. NIMS observation e4i007tr measured radiance at 96
 101 wavelengths across the full NIMS range. The five usable nighttime observations were obtained
 102 at ranges from 752,083 km to 905,805 km, yielding spatial resolutions from 376 to 453 km/pixel,
 103 and at emission angles of 69.4° to 77.8°. Spectral resolution was low, with measurements at 10
 104 to 12 wavelengths spread evenly across the NIMS wavelength range. Poor spectral resolution is
 105 problematic as radiation-induced spikes in the NIMS data are often detectable by their deviation
 106 from other data close by in the spectrum. Also, problems with NIMS detectors 1 and 2 ($< 1 \mu\text{m}$)
 107 render these data unreliable. Where data have been fitted with the black-body thermal emission
 108 model (see below), an effort was made to ensure that most data fall on or below the resulting
 109 curve to maximize the integrated thermal emission (Davies, 2003). The uncertainty of the de-
 110 spiking and the inherent scatter within the e4i006tr and e4i025tr data reduces confidence in the
 111 temperature derivations such that a strong constraint on lava eruption temperature is not possible.
 112 However, the present analysis is based on the comparison of the overall shape of the thermal
 113 emission spectra and relative intensity of thermal emission from observation to observation,
 114 tasks for which the data are well suited. There was no clear detection of Marduk Fluctus in
 115 another nine observations obtained during E4 at high emission angles and low spatial resolution,
 116 especially where data were so heavily impacted by radiation as to render them unusable. Usable
 117 NIMS E4 Marduk Fluctus nighttime data are shown in Figure 3a.



118

119 **Figure 3a.** Radiances from Marduk Fluctus (symbols) and thermal emission model spectra (solid lines) synthesized from the best two-temperature, two-area fits to the data using the temperatures
 120 and areas in Table 1. The numbers refer to the order in which the observations were obtained.
 121 Data are corrected for emission angle. The intervals between observations are also shown.
 122



123

124 **Figure 3b.** Radiances uncorrected for emission angle e (solid lines). The lower boundary of
 125 thermal emission is obtained by subtracting the pre-event e -corrected e4i006tr radiance (1) from
 126 the uncorrected radiance spectra from the “explosion” observations (e4i017tr, e4i018tr and
 127 e4i019tr, denoted by 2', 3' and 4').

128 3 Methods

129 NIMS radiance data are processed by adding radiances from adjacent pixels to account for the
 130 NIMS point-spread function (e.g., Davies, 2007). Obvious radiation-induced spikes are
 131 removed. An emission angle correction is applied. If the thermal emission source was
 132 essentially a flat plate (a broad lava flow or a lava lake surface), and thermal emission was
 133 Lambertian, then dividing the radiances by the cosine of the emission angle would be appropriate
 134 to determine the actual emitting areas and thermal emission. However, as lava flows are not
 135 two-dimensional and thermal emission can be detected at emission angles $\gg 70^\circ$, then the cosine
 136 correction may exaggerate the power and area of the thermal source. Additionally, if the thermal
 137 source was above the surface – a lava fountain, for example, or clasts from an explosion – then a
 138 cosine correction should not be applied. The suitability of applying the cosine correction in this
 139 particular case is discussed below. The NIMS data are fitted with a two-temperature, two-area
 140 (“2-T, 2-A”) model (e.g., Davies et al., 1997; 2001). The model minimizes the residuals between
 141 the data and the model output. The resulting relatively small, hot area is the sum of the hot vent
 142 (if present), young lava surfaces including new lava breakouts, lava fountains, incandescent open

143 channel flows, and areas within a lava lake or pond where the crust is being disrupted. The
144 lower temperature component, a much larger area in these cases, corresponds to the cooling and
145 insulating crust that forms on lava flows and lava lakes.

146 **4 Results**

147 The NIMS data are mostly well constrained by the “2-T, 2-A” model. Figure 3 shows the
148 evolution of the thermal event. Data are processed in three ways to account for uncertainty in the
149 vertical extent of the lava (and hence the appropriate emission angle correction to use), and all
150 three processed datasets are fitted with the 2T, 2A model (Table 1). Firstly, all data are corrected
151 for emission angle. This represents the upper limit of thermal emission. Secondly, the data
152 showing the thermal spike (e4i017tr, e4i018tr and e4i019tr) are left uncorrected for emission
153 angle; and thirdly, the thermal spike data are not corrected for emission angle and have the
154 emission angle corrected e4i007tr “pre-event” spectrum subtracted. This isolates the spike’s
155 thermal component from the background and is the lower boundary of the event’s thermal
156 emission. The resulting spectra are shown in Figure 3b.

157 Considering data that have been corrected for emission angle, at some time in the 136 minutes
158 between observations e4i006tr and e4i017tr, thermal emission increased by more than an order
159 of magnitude at all wavelengths. In the next two minutes and two seconds, between e4i017tr and
160 e4i019tr, thermal emission decreased rapidly, mostly at wavelengths between 3.5 and 5.2 μm .
161 There was an increase in the peak of thermal emission from 2.7 μm for e4i017tr, suggesting an
162 effective brightness temperature T_{eff} of 1035 K to 2.4 μm for e4i018tr ($T_{\text{eff}}=1207$ K) to 1.8 μm
163 for e4i019tr ($T_{\text{eff}}=1610$ K). As two-temperature, two-area fits may underestimate the
164 temperature of the hottest areas present, the actual eruption temperature may be well in excess of
165 1600 K, which would suggest an ultramafic lava composition. Over the same time interval, the
166 hot component area tracks the rise and fall of thermal emission starting at a fraction of a km^2 ,
167 rising to an area of 11 km^2 , then rapidly decaying to an area of less than 1 km^2 again. After
168 another 23 minutes, thermal emission across short NIMS wavelengths has dropped to below the
169 pre-event background level at short NIMS wavelengths.

170 However, at wavelengths longer than 4 μm , a slope develops in the data suggesting an additional
171 larger, cool component is present, one that was not present in the e4i006tr observation. The
172 measured spectral radiance demonstrates a shift in the peak in thermal emission to longer
173 wavelengths (suggesting a lower temperature) from e4i019tr to e4i025tr. The e4i019tr data
174 suggest a rapidly dwindling hot area and a new, large, cool area that is still detectable in the
175 e4i025tr data. We note that the model fits to the e4i019tr and e4i025tr data are poorly
176 constrained because of scatter of the sparse data. It is apparent that some of the data are
177 impacted by noise. We do not know which points are the noisy ones. Fitting the upper boundary
178 of the e4i025tr data yields a cool area of 10,000 km^2 at 290 K. This might be a cool plume or
179 blanket of small pyroclastics resulting from the explosion. We can only speculate as to what this

180 may represent. The lack of a 200-km diameter low-albedo (silicate-rich) deposit in subsequent
181 *Galileo* imagery suggests that this deposit either does not exist or was buried under later, higher-
182 albedo, sulfur-rich plume fallout. Fitting by weighting the lower data points between 3.5 and 5.2
183 μm yields a smaller cool component area covering 190 km^2 at 395 K. In any event, the low level
184 of thermal emission in e4i025tr shows rapid cooling, consistent with the explosion hypothesis
185 discussed below.

186 **5 Discussion**

187 The radiance from this event, with such rapid waxing and waning in radiance at all wavelengths
188 and with such large variations in intensity, changes more rapidly than has been previously seen
189 on Io (Blaney et al., 1995; Davies, 1996; Sinton et al., 1983). We can speculate as to what
190 physical process generates this thermal signal evolution. The increase in short wavelength
191 thermal emission can be explained by the exposure of incandescent lava erupting at temperatures
192 well in excess of 1000 K. This could be caused by a new outbreak of lava, a lava fountain
193 issuing from a fissure, fountaining in a lava lake, or the rapid overturning and replacement of
194 crust in a lava lake; all of these processes generate strong increases in short wavelength thermal
195 emission (Davies et al., 2010). However, the E4 thermal spike is unique with the thermal
196 emission returning to the pre-event level very quickly (a few minutes). Newly exposed
197 incandescent lava initially cools very rapidly, but the rate of cooling decreases as temperature
198 decreases. On Io, basalt cools from 1475 K to 1100 K in about a minute and to 1020 K in two
199 minutes, but it takes another 1.6 hours to cool to 700 K and another 32 hours to cool to 500 K
200 (Davies, 1996). The thermal signal in the E4 data reached the pre-event background level in no
201 more than 23 minutes (the time between e4i017tr and e4i025tr). A replaced crust on a lava lake
202 does not cool fast enough to explain the data. The eruption of a new lava flow would have to be
203 very brief ($<$ a few minutes) and still cover multiple km^2 before abruptly stopping – and would
204 still not cool fast enough to depress the thermal emission to the observed post-event level.

205 The observations were obtained at high emission angles, and so thermal emission from the
206 surface may be blocked by topography (e.g., de Kleer and de Pater, 2017; Radebaugh et al.,
207 2002). The emission angle changed from 69.4° to 77.8° during the five E4 observations. The
208 “background” level of thermal emission does decrease slightly at short wavelengths after the
209 thermal event, but the emission angle difference is $<2^\circ$ from that of the peak of the eruption and
210 so topographic control is unlikely. The thermal emission from the Marduk Fluctus lavas, likely
211 from lava flows dominated by a relatively cool insulating crust, is visible at high emission angles
212 and is therefore not shielded by topography. Likewise, if the thermal emission from Marduk
213 Fluctus is emanating from a lava lake, then the lava lake surface is not topographically shielded
214 either. Of the 40 other NIMS observations of this area, the thermal emission at $5 \mu\text{m}$ is constant
215 at about $15 \pm 6 \text{ GW}/\mu\text{m}$ over a wide range of emission angles (excluding the E4 thermal event
216 data). The E4 data cannot be explained simply by the emplacement of a new lava flow or the
217 quiescent replacement of the crust in a lava lake.

218 The E4 event had to be caused by a different style of activity. We propose that this event was a
219 short-duration eruption event – a strombolian or vulcanian explosion. It is unlike most terrestrial
220 strombolian activity in as much as this appears to be a single event, and terrestrial strombolian
221 eruptions are episodic. However, poor temporal resolution over much of the duration of the
222 *Galileo* mission may have prevented other similar events from being detected; alternatively other
223 such events simply have not yet been identified in the NIMS data.

224 Strombolian events are driven by the abrupt release of gas that has accumulated within the
225 ascending magma when the pressure becomes too great to be contained. On Io, as magma
226 ascends through the lithosphere, it can thermally interact with interbedded layers of pyroclastic
227 material, lava flows and plume deposits rich in SO₂ and sulfur, and may therefore add volatiles to
228 any primary volatiles already present in the magma (Leone et al., 2011).

229 Such explosions have been observed in the phonolite lava lake of Erebus volcano, Ross Island,
230 Antarctica (e.g., Gerst et al., 2013). The contents of the lava lake, which in December 2005 was
231 38 m across (Davies et al., 2008), were entirely evacuated and disrupted into fragments. These
232 fragments, ranging in size typically from mm to in excess of 1 m in diameter are ejected at
233 velocities often exceeding 50 m/s (Gerst et al., 2013). In 2005-2006, bombs were distributed as
234 far as 600 m from the lava lake (Gerst et al., 2008), and explosions occurred every 6 to 9 hours.
235 After such an explosion, the lava lake quickly refilled and within a few minutes (as witnessed by
236 the lead author), appeared as it did before the explosion.

237 An explosion in a lava lake can also be caused by the fall of material from the crater wall into the
238 lava lake. This has been observed repeatedly at the lava lake that began forming in 2008 in
239 Halema'uma'u, Kilauea volcano, Hawai'i. The lava lake enlarges through failure of the
240 undermined walls of the pit in which it resides. Rockfall into the lake apparently triggers the
241 abrupt release of volatiles in lava close to the surface, possibly by runaway decompressive
242 vesiculation, leading to an explosion (Orr et al., 2013). The explosion, possibly exacerbated by
243 the formation of a rebound-splash Worthington jet (Orr et al., 2013), and the generation of an ash
244 cloud that includes juvenile tephra, is followed by powerful roiling of the lava until equilibrium
245 is restored. Eventually, the lava lake surface temperature distribution returns to pre-eruption
246 levels.

247 On Io, such a gas-driven explosion would be enhanced by the environment. The lack of a
248 substantial atmosphere allows unrestrained expansion of the gas, increasing the fragmentation of
249 the lava and increasing ejection velocity over a similar eruption on Earth. The lower gravity on
250 Io increases the range (Wilson and Head, 1983).

251 Phreatomagmatic activity can also cause explosions on basaltic volcanoes. A rootless explosion
252 may be caused by the thermal mobilization of surface ices underneath a thick lava flow. Such an
253 explosion was observed during the Eyjafjallajökull, Iceland eruption in 2010 (A. Hoskuldsson,

254 pers. comm. 2010). In 1924 and 2008, ground water interacting with hot rock caused ash-rich
255 explosions on Kilauea volcano, Hawai'i (e.g., Houghton et al., 2011; Mastin, 1997).

256 Rather than being strombolian, the explosion may be vulcanian in nature. Although vulcanian
257 eruptions are generally associated with more viscous lava than basalt, the collection of gas-rich
258 lava under the cooled crust of a lava lake or lava flow could build up pressure to the point that an
259 explosion occurs.

260 An explosion of some kind best explains the *Galileo* orbit E4 NIMS Marduk Fluctus data. A
261 powerful explosion would generate clasts that, if very small, would cool rapidly. On Io, a basalt
262 clast of radius 1 mm would cool from 1480 K to 700 K in less than a minute (Keszthelyi et al.,
263 2007), and would cool to 520 K in two minutes and to 290 K in just over 12 minutes. The
264 explosive generation of small clasts, initially erupted at a liquidus temperature at or above 1400
265 K, would generate the observed thermal spike and subsequent rapid thermal decay as the clasts
266 were widely dispersed and rapidly cooled. Similar small clasts formed during lava fountaining
267 events that took place on the early Moon (Wilson and Head, 1981; 1983).

268 The emitted power P from each clast = $4\pi R^2 \sigma T^4$, where R is the clast radius, T is absolute clast
269 temperature, and σ is the Stefan-Boltzmann constant ($5.67 \times 10^{-8} \text{ W m K}^{-4}$). If $R = 0.001 \text{ m}$ and
270 $T = 1400 \text{ K}$, $P = 2.73 \text{ W}$ per clast. Estimates of radiated power from the event during e4i017tr
271 are 1735 GW (cosine-corrected data); 256 GW (uncorrected data); and 29 GW (uncorrected,
272 subtracting corrected e4i006tr data). Each clast has a volume of $4.12 \times 10^{-9} \text{ m}^3$ and a mass of
273 $1.09 \times 10^{-5} \text{ kg}$, assuming a density of 2600 kg m^{-3} . Assuming we see radiation from half the
274 clasts present, the volume of material ejected spans 89 to 5310 m^3 (mass = 2.31×10^5 to $1.38 \times$
275 10^7 kg). These volumes are orders of magnitude smaller than the volumes erupted ($6\text{-}13 \text{ km}^3$)
276 from larger, longer duration fire fountain eruptions elsewhere on Io (Davies et al., 2001; de Pater
277 et al., 2014a).

278 Given the low spatial resolution of the data, it is not known with certainty if the eruption took
279 place exactly at Marduk Fluctus, within Marduk Patera, or nearby. Rata Patera, another active
280 volcano detected by NIMS, is located at 200°W , 36°S , and may contribute to the observed
281 radiance in the high emission angle data. Nevertheless, Marduk Fluctus seems to be the most
282 likely candidate, based on the constancy of thermal emission as seen in these and higher spatial
283 resolution data. Regardless of exactly where this event took place, the detection of this style of
284 activity means that another volcanic process has been identified that designers of future Io
285 instruments and missions need to be aware of as a suitable target for determining the eruption
286 temperature of Io's silicate lava. Such observations would require unsaturated data of such
287 events to be acquired simultaneously (or within $\approx 0.04 \text{ s}$ – Davies et al., 2011; 2017) at multiple
288 visible and/or infrared ($\leq 1.5 \mu\text{m}$) wavelengths. The chances of observing future events are good
289 as this was a powerful eruption identified in low spatial resolution data at a great distance from
290 Io. We are currently searching for similar hidden gems in the NIMS dataset.

291 **Summary**

292 This explosive event evolved on a much faster time scale than other volcanic processes observed
293 by NIMS, and occurred on a shorter timescale and smaller areal scale than the much larger and
294 more powerful “outburst” eruptions, characterized by fountains feeding lava flows (Davies et al.,
295 2001). This smaller class of outburst-like eruptions may be more common (de Kleer and de
296 Pater, 2016) than outbursts. We note that the temporal resolution of the NIMS data,
297 extraordinary as it is, leaves open the possibility that the peak of thermal emission was not seen.
298 NIMS constrains the onset of the event to within \approx two hours. We do not know how big this
299 event might have been, or how rapid the waxing phase was – but we do observe that the thermal
300 source decayed quickly (in a few minutes). Such an event may be appropriate for determining
301 lava eruption temperature by instruments on spacecraft, even at hundreds of thousands of
302 kilometers from Io, if correctly imaged.

303 **Acknowledgments**

304 This work was performed at the Jet Propulsion Laboratory-California Institute of Technology,
305 under contract to NASA. AGD thanks the NASA Outer Planets Research and Planetary Geology
306 and Geophysics Programs for past support under awards NNN13D466T and NMO710830. The
307 research was partially supported by the National Science Foundation, NSF grant AST-1313485
308 to UC Berkeley. LW thanks the Leverhulme Trust for an Emeritus Fellowship. NIMS data are
309 available from the NASA Planetary Data System. © Caltech 2018.

310

311

312

Table 1. Characteristics of NIMS E4 observations including Marduk Fluctus and boundary two-temperature, two-area model fits.

Observation	Observation id	Date, time	No. of NIMS λ	Range	Emission angle	Temp 1	Area 1	Temp 2	Area 2	Power area 1	Power area 2	Total power ^a
				km	°	K	km ²	K	km ²	GW	GW	GW
e4i007tr (1)	E4INHRSPEC01 ^b	12/18/96 21:29	96	319480	24.3	284	3600	-	-	1328	-	1328
e4i006tr (1)	E4INCOOLCV02C	12/19/96 13:40	10	752083	69.4	1400	0.2	440	100	44	213	256
e4i017tr (1)	E4INWARMCV03A	12/19/96 15:56	10	880418	76.4	1144	10.8	496	201	1047	689	1735
e4i017tr (2)	E4INWARMCV03A	12/19/96 15:56	10	880418	76.4	1144	2.52	496	46.9	245	161	406
e4i017tr (3) ^c	E4INWARMCV03A	12/19/96 15:56	10	880418	76.4	1085	2.71	-	-	212	-	212
e4i018tr (1)	E4INWARMCV03B	12/19/96 15:57	10	881752	76.5	1332	4.2	567	142	741	834	1575
e4i018tr (2)	E4INWARMCV03B	12/19/96 15:57	10	881752	76.5	1332	0.98	567	33	175	193	368
e4i018tr (3)	E4INWARMCV03B	12/19/96 15:57	10	881752	76.5	1368	0.49	899	2.22	98	82	180
e4i019tr (1)	E4INWARMCV03C	12/19/96 15:58	10	882869	76.5	1722	0.5	714	15.0	238	221	459
e4i019tr (2)	E4INWARMCV03C	12/19/96 15:58	10	882869	76.5	1722	0.12	714	3.5	60	52	112
e4i019tr (3) ^c	E4INWARMCV03C	12/19/96 15:58	10	882869	76.5	1800	0.05	-	-	29	-	29
e4i025tr (1)	E4INWARMCV04A	12/19/96 16:21	10	905805	77.8	830	1.4	290	1x10 ⁴	38	4010	4048
e4i025tr (2)	E4INWARMCV04A	12/19/96 16:21	10	905805	77.8	830	0.29	290	2133	8	847	855

Notes:

a An emissivity e of 1 is used.b e4i007tr temperature and area derived from 4.999 μm radiance of 17.26 GW/ μm from an area of 3600 km² (Veeder et al., 2012).

c Data best fitted with single component.

(1) Model fits to data corrected for emission angle.

(2) Model fits to “explosion” data not corrected for emission angle.

(3) Model fits to “explosion” data not corrected for emission angle, having subtracted emission angle corrected e4i006tr data.

References

- Becker, T., Geissler, P. E., 2005. *Galileo* Global Color Mosaics of Io. 36th Lunar and Planetary Science Conference. abstract 1862, on CD-ROM.
- Belton, M. J. S., et al., 1996. *Galileo's* First Images of Jupiter and the Galilean Satellites. *Science*. 274, 377-385.
- Blaney, D. L., Johnson, T. V., Matson, D. L., Veeder, G. J., 1995. Volcanic eruptions on Io: Heat flow, resurfacing, and lava composition. *Icarus*. 113, 220-225.
- Carlson, R. W., Weissman, P. R., Smythe, W. D., Mahoney, J. C., 1992. Near-Infrared Mapping Spectrometer experiment on *Galileo*. *Space Science Reviews*. 60, 457-502.
- Davies, A. G., 1996. Io's Volcanism: Thermo-Physical Models of Silicate Lava Compared with Observations of Thermal Emission. *Icarus*. 124, 45-61.
- Davies, A. G., 2003. Volcanism on Io: Estimation of eruption parameters from *Galileo* NIMS data. *J. Geophys. Res. (Planets)*. 108, 5106-5120.
- Davies, A. G., 2007. Volcanism on Io: a comparison with Earth. Cambridge University Press, Cambridge, 376 pages.
- Davies, A. G., et al., 2008. Multi-Instrument Remote and *In-Situ* Observations of the Erebus Volcano (Antarctica) Lava Lake in 2005: a Comparison with the Pele Lava Lake on the Jovian Moon Io. *J. Volcanol. Geoth. Res.* 177, 705-724.
- Davies, A. G., Keszthelyi, L., McEwen, A. S., 2011. Estimating Eruption Temperature From Thermal Emission Spectra of Lava Fountain Activity in the Erta' Ale (Ethiopia) Volcano Lava Lake – Implications for Observing Io's Volcanoes. *Geophys. Res. Lett.* 38, L21308.
- Davies, A. G., Keszthelyi, L. P., Harris, A. J. L., 2010. The Thermal Signature of Volcanic Eruptions on Io and Earth. *Journal of Volcanology and Geothermal Research*. 194, 75-99.
- Davies, A. G., Keszthelyi, L. P., McEwen, A. S., 2016. Determination of Eruption Temperature of Io's Lavas Using Lava Tube Skylights. *Icarus*. 278, 266-278.
- Davies, A. G., et al., 2001. Thermal signature, eruption style, and eruption evolution at Pele and Pillan on Io. *Journal of Geophysical Research*. 106, 33079-33104.
- Davies, A. G., et al., 2017. A novel technology for measuring the eruption temperature of silicate lavas with remote sensing: Application to Io and other planets. *J. Volcanology and Geothermal Research*. 343, 1-16.
- Davies, A. G., Veeder, G. J., Matson, D. L., Johnson, T. V., 2012. Io: Charting thermal emission variability with the *Galileo* NIMS Io Thermal Emission Database (NITED): Loki Patera. *Geophysical Res. Letters*. 39, L01201, doi:10.1029/2011GL049999.
- de Kleer, K., de Pater, I., 2016. Time variability of Io's volcanic activity from near-IR adaptive optics observations on 100 nights in 2013–2015. *Icarus*. 280, 378-404.
- de Kleer, K., de Pater, I., 2017. Io's Loki Patera: Modeling of Three Brightening Events in 2013-2016. *Icarus*. 289, 181-198.
- de Pater, I., Davies, A. G., Adamkovics, M., Ciardi, D. R., 2014a. Two New, Rare, High-Effusion Outburst Eruptions at Rarog and Heno Paterae on Io. *Icarus*. 242, 365-378.
- de Pater, I., et al., 2014b. Global Near-IR Maps from Gemini-N and Keck in 2010, with a Special Focus on Janus Patera and Kanehekili Fluctus. *Icarus*. 242, 379-395.
- Gerst, A., Hort, M., Kyle, P. R., Vöge, M., 2008. 4D velocity of Strombolian eruptions and man-made explosions derived from multiple Doppler radar instruments. *Journal of Volcanology and Geothermal Research*. 177, 648-660.

- Gerst, A., M. Hort, R. C. Aster, J. B. Johnson, Kyle, P. R., 2013. The first second of volcanic eruptions from the Erebus volcano lava lake, Antarctica—Energies, pressures, seismology, and infrasound. *J. Geophys. Res. Solid Earth*. 118, 3318–3340.
- Houghton, B. F., Swanson, D. A., Carey, R. J., Rausch, J., Sutton, A. J., 2011. Pigeonholing pyroclasts: Insights from the 19 March 2008 explosive eruption of Kilauea volcano. *Geology*. 39, 262-266.
- Keszthelyi, L., Jaeger, W., Milazzo, M., Radebaugh, J., Davies, A. G., Mitchell, K., 2007. New estimates for Io eruption temperatures: implications for the interior. *Icarus*. 192, 491-502.
- Keszthelyi, L., et al., 2001. Imaging of volcanic activity on Jupiter's moon Io by *Galileo* during the *Galileo* Europa Mission and the *Galileo* Millennium Mission. *J. of Geophys. Res.* 106, 33025-33052.
- Leone, G., Wilson, L., Davies, A. G., 2011. The geothermal gradient of Io: consequences for lithosphere structure and volcanic eruptive activity. *Icarus*. 211, 623-625.
- Lopes-Gautier, R., et al., 1997. Hot spots on Io: Initial results from *Galileo*'s near infrared mapping spectrometer. *Geophysical Research Letters*. 24, 2439.
- Mastin, L. G., 1997. Evidence for water influx from a caldera lake during the explosive hydromagmatic eruption of 1790, Kilauea Volcano, Hawai'i. *Journal of Geophysical Research*. 102, 20,093–20,109.
- McEwen, A. S., et al., 1998. High-Temperature Silicate Volcanism on Jupiter's Moon Io. *Science*. 281, 87-90.
- McEwen, A. S., et al., 1997. High-temperature hot spots on Io as seen by the *Galileo* Solid State Imaging (SSI) experiment. *Geophysical Research Letters*. 24, 2443-2446.
- Orr, T., Thelin, W. A., Patrick, M. P., Swanson, D. A., Wilson, D. C., 2013. Explosive eruptions triggered by rockfalls at Kilauea volcano, Hawai'i. *Geology*. 41, 207-210.
- Radebaugh, J., McEwen, A. S., Milazzo, M., Davies, A. G., Keszthelyi, L. P., Geissler, P., 2002. *Galileo* SSI and Cassini ISS Observations of Io's Pele Hotspot: Temperatures, Areas, and Variation with Time. *Lunar and Planetary Institute Conference Abstracts*, Vol. 33, pp. 1445.
- Sinton, W. M., Lindwall, D., Cheigh, F., Tittlemore, W. C., 1983. Io - The near-infrared monitoring program, 1979-1981. *Icarus*. 54, 133-157.
- Strom, R. G., Schneider, N. M., Terrile, R. J., Cook, A. F., Hansen, C., 1981. Volcanic eruptions on Io. *Journal of Geophysical Research*. 86, 8593-8620.
- Veeder, G. J., Davies, A. G., Matson, D., Johnson, T. V., Williams, D. A., Radebaugh, J., 2012. Io: Volcanic Thermal Sources and Global Heat Flow. *Icarus*. 219, 701-722.
- Veeder, G. J., Davies, A. G., Matson, D. L., Johnson, T. V., 2009. Dark Flow Fields on Io. *Icarus*. 204, 239-253.
- Wilson, L., Head, J. W., 1981. Ascent and eruption of basaltic magma on the Earth and Moon. *Journal of Geophysical Research*. 86, 2971-3001.
- Wilson, L., Head, J. W., 1983. A comparison of volcanic eruption processes on Earth, Moon, Mars, Io and Venus. *Nature*. 302, 663-669.